international journal of aeroacoustics volume 9 · number 4 & 5 · 2010 – pages 533–558

Wave-packet models for large-scale mixing noise

Ramons Reba*, Satish Narayanan† and Tim Colonius‡

*,† *United Technologies Research Center, E. Hartford, CT*

‡ *California Institute of Technology, Pasadena, CA*

December 17, 2009

ABSTRACT

A wave-packet Ansatz is used to model jet noise generation by large-scale turbulence. In this approach, an equivalent source is defined based on the two-point space-time correlation of hydrodynamic pressure on a conical surface surrounding the jet plume. The surface is sufficiently near the turbulent flow region to be dominated by non-propagating hydrodynamic signatures of large-scale turbulent structures, yet sufficiently far that linear behavior can be assumed in extending the near-field pressure to the acoustic field. In the present study, a 78-microphone array was used to measure hydrodynamic pressure on the conical surface in order to identify parameters for the model and to validate the approach. Six microphones were distributed in the azimuthal direction at each of 13 axial locations spanning the first 8 jet diameters, allowing decomposition of azimuthal modes $m = 0$ and $m = 1$. We show that a source model based on a Gaussian correlation function provides a consistently good representation of the noise source attributed to large-scale structures. The results provide evidence that large-scale wave-like structures, known to dominate aft radiation at supersonic phase speeds, are also relevant at subsonic speeds.

1. INTRODUCTION

Jet noise has been a topic of research interest over the past sixty years, motivated by the need to reduce aircraft noise in the face of increasingly stringent environmental regulations. As a result, many aspects of jet noise are now well understood. However, the fundamental mechanisms of turbulent jet mixing noise remain topics of debate. In particular, models for noise generation associated with the (controllable) dynamics of

*Research Engineer, Thermal & Fluid Sciences Department.

†Project Leader, Fire and Security Program Office.

‡Professor, Mechanical Engineering.

large-scale, coherent flow structures are absent. In addition, there is no comprehensive theory enabling jet noise prediction from first principles. Although methods such as Large Eddy Simulation (LES) [1] have made enormous strides, these tools are still prohibitively time consuming for routine engineering applications, and by themselves do not readily reveal fundamental source mechanisms. Arguably, this incomplete understanding is an impediment to conceiving new, more effective, jet noise control strategies.

Early advances in jet noise theory were based on Lighthill's Acoustic Analogy [2] and its extension by Lilley [3] to include flow-acoustic interaction in the propagation operator. Lilley's Equation formed the basis of the first jet noise prediction methodology [4] to be adopted by industry, and recent efforts have focused on improving models for the equivalent sources using data from Reynold's Averaged Navier-Stokes (RANS) calculations [5, 6]. Approaches using equivalent source descriptions not based on the Lighthill/Lilley Analogies have also been developed [7, 8]. The above models have proven very successful in predicting jet mixing noise at angles near 90° to the jet axis, but have generally been unsuccessful in predicting aft-radiated noise.

As an alternative to acoustic analogy based theories, many researchers have pursued phenomenological models based on the concept of large-scale turbulent structures with wave-like descriptions. Mollo-Christensen [9] measured pressure fluctuations in the near-field of a turbulent jet, and suggested a wave-packet Ansatz for the observed orderly structure. This source description parallels the association of large-scale structures with instability waves, as pursued by Liu and Mankbadi [10, 11, 12], and Morris, Giridharam, and Lilley [13]. For jets with supersonic turbulence convection speeds, it is well understood that such structures generate noise in the form of direct Mach wave radiation, analogous to that produced by a supersonically convecting 'wavy wall', as discussed by Tam [14]. Noise models based on linear, supersonically convecting instability waves have been developed for mixing-layers [15, 16] and axisymmetric jets [17], and more recent studies have addressed Mach wave radiation from non-linearly evolving instabilities [18].

At subsonic convection speeds, the relevance of wave-like structures for noise generation has been debated, since the direct Mach wave radiation process is absent, and generation of wavenumbers with supersonic phase speeds relies on subtleties of the wave growth and decay. Through an exhaustive investigation of far-field jet measurements Tam, Golebiowski and Seiner [19] showed that at aft angles, both subsonic and supersonically convecting jets exhibit similar characteristic spectral shapes. This has led to the postulate that large-scale wave-like structures, known to dominate aft radiation at supersonic phase speeds, are an equally relevant source at subsonic speeds. Several recent studies have provided experimental evidence and analysis to further support this idea [20, 21].

Numerous approaches for identifying source mechanisms in jets have been pursued over the years. These include simultaneous measurements of far-field sound and in-flow velocity, density, or pressure fluctuations [22, 23, 24, 25] aiming to establish a direct cause-and-effect relationship between turbulence characteristics and noise, and advanced particle-image velocimetry (PIV) techniques for mapping multi-point velocity statistics [26, 27]. Other studies [28, 29] have used simultaneous acoustic measurements

and (scalar) visualizations of the flow field to provide insight into the evolution of large-scale flow structures and their relation to peak noise generation.

In recent years, the jet near-field pressure has received renewed attention. Arndt et al. [30] applied proper orthogonal decomposition (POD) to the near-field hydrodynamic pressure to educe coherent structures in a turbulent jet. By applying POD to jet simulation data, Freund and Colonius [31, 32] showed that the pressure signatures of coherent flow features exhibit a distinctive wave-packet structure in subsonic jets. Ukeiley and Ponton [33] characterized the dynamic and three-dimensional nature of pressure signatures over a spatially extended jet region and speculated the connection between lower azimuthal mode number structures at low frequencies and the far-field noise. Picard and Delville [34] applied POD and linear stochastic estimation (LSE) to estimate the acoustic source using limited measurements of near-field pressure and velocity fluctuations. By applying Lighthill's Analogy, the result was used to estimate the radiated sound. A similar approach, using more extensive PIV measurements was used by Tinney et al. [35] to provide a low-dimensional description of noise producing flow events, and to compute their sound radiation. Kerherve et al. [36] and Tinney et al. [37] used structure eduction methods in combination with wavenumber-frequency filtering to identify acoustically significant features in the jet near field. By adapting microphone array beam-forming techniques, Suzuki and Colonius [38] quantified near-field pressure wave-packets in terms of linear instability waves.

For very low Mach number flows, Crighton and Huerre [39] considered a model wave-packet problem to elucidate the superdirective nature of noise radiation and its dependence on the shape (i.e. algebraic, exponential, Gaussian) and size of the wave packet envelope (inferred from the near-field pressure measurements of Laufer and Yen [40]). Motivated by pressure correlation measurements by Fuchs [41], Michalke [42] analytically investigated the effect of axial source coherence on noise generation using an assumed Gaussian envelope function. It was shown that as the jet convection Mach number increases to unity, noise radiation intensifies with increasing source coherence (relative to a length scale based on the source volume).

In this paper, we adopt an approach inspired by the above studies, and construct a semi-empirical wave-packet source model for mixing noise from large-scale turbulent structures. Our approach is based on the concept of measuring pressure statistics just outside the jet shear layer to capture signatures of the large-scale turbulence. Microphones are configured to be sufficiently near the turbulent flow region to capture flow signatures, yet far enough that non-linear source terms can be neglected. Under these conditions, the linear wave equation describes both signatures of the flow structure (the source) and the acoustic wave propagation. It follows that the linear wave equation can be used to 'project' the source pressure to the acoustic field, and thereby relate dynamics of large-scale turbulence to noise generation. The equivalent noise source defined here is described by second order statistics of a scalar quantity (pressure), rather than fourth-order statistics of a vector quantity over a volume as required by more conventional acoustic analogies. Although the source description adopted here is less fundamental than that of Lighthill or Lilley, it can be measured experimentally with relative ease.

The work described here relies on a simple analytical model motivated by experimental measurements, and in its present form does not provide a first-principles predictive capability. However, the beam-forming results of Suzuki and Colonius [38] demonstrated that eigenfunctions obtained from stability analysis well represent the coherent flow structures from the nozzle exit to the end of the potential core, particularly near the most amplified frequency of each azimuthal mode. This observation provides a theoretical motivation for the current wave-packet description, and offers promise that by using stability-based methods, the current framework may lead to a predictive capability suited for analysis and design of nozzles of technological interest.

In the following, we first describe the experimental facility and method. This is followed by a description of the acoustic projection method to link measured near-field source characteristics to the far field. Finally, the acoustic field is re-constructed from the measured equivalent source, and compared against measurements.

2. EXPERIMENTAL FACILITY AND METHOD

We briefly describe salient details of the experimental method; further details regarding the microphone array measurements are given in references [38] and [43]. The experiments were conducted using the Small Hot Jet Acoustic Rig (SHJAR) [44] at NASA Glenn Research Center. A single-stream round jet issued from a converging nozzle with exit diameter D of 5.08 cm (2.0 inches). The nozzle was mounted 3.05 m from the ground in an anechoic dome with a 20 m radius. Experiments were conducted at a variety of set points from the matrix of Tanna [45]. PIV measurements were previously made in in-flow and cross-flow planes [27].

Quarter-inch Bruel & Kjaer microphones were placed in two conical array configurations depicted in figure 1, and data was acquired at a sampling rate of 50 kHz. In the first case (figure la), a 78 microphone array was placed just outside the jet mixing layer to measure the hydrodynamic pressure associated with large-scale turbulent structures (instability waves). The array location and microphone spacing were designed by Suzuki & Colonius [38] based on linear stability analysis of the jet mean flow fields (from PIV) in order to detect instability waves over a range of low frequencies and azimuthal mode numbers from 0 (axisymmetric) to 2. The array has 13 rings with $0.625D$ inter-ring spacing and a total axial extent just over $8D$. Six microphones are placed on each ring with an equal spacing of 60°; microphones are staggered in the azimuthal direction by an amount of 30° at every other ring. The spacing and axial positions were determined to allow just 7 rings of microphones to span approximately two instability wavelengths. The spreading angle of the array (cone half angle) is 11.3°, determined to be slightly wider than the spreading of the velocity fluctuations. The error in microphone position was estimated to be less than $0.05D$ from a noise-source test using a spark plug. This error is at most 5% of the instability wavelength. The background noise amplitude was at least three orders of magnitude smaller than signals from the jet.

The second array (figure 1b) was designed by James Bridges (NASA Glenn) to measure the acoustic field. Microphones were placed in the range of $17.3D < r < 25D$, which is about 2 to 3 wavelengths of sound at the peak frequency, and is therefore in the

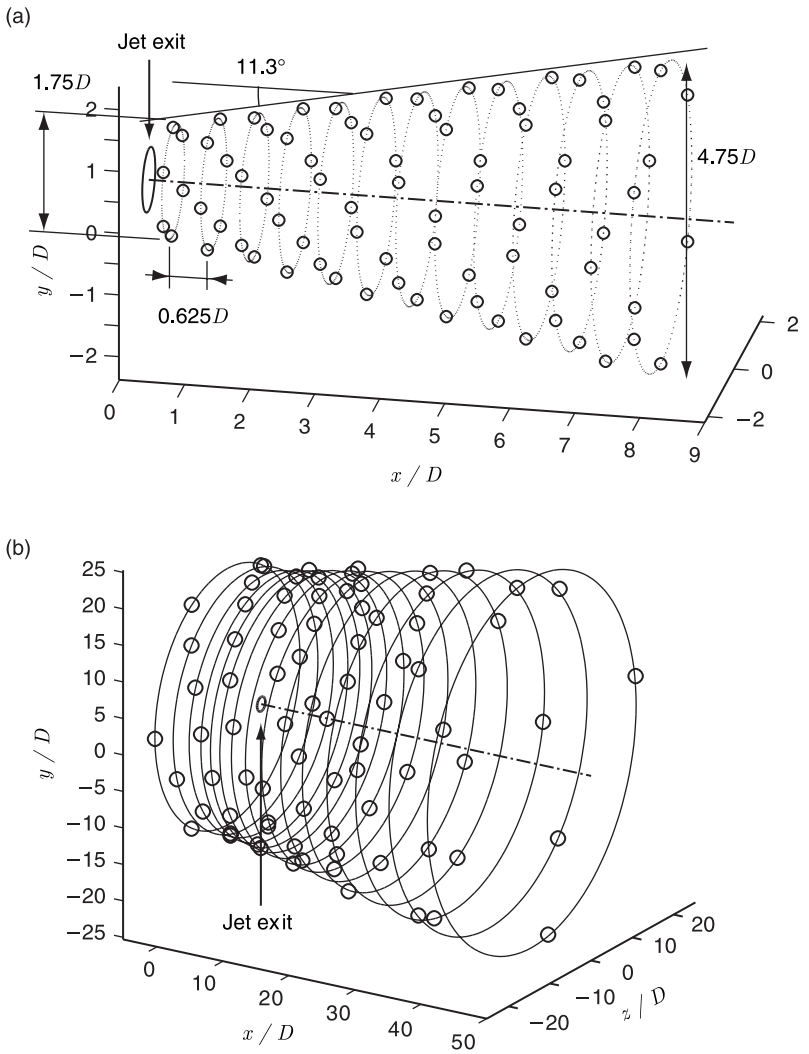

Figure 1: Microphone distributions of (a) near-field hydrodynamic array and (b) acoustic array.

acoustic mid-field. The array covers polar angles in the acoustic field (measured from the downstream direction) of 31.7° to 106.3°. Fifteen axial ring positions were designed to give nearly equally spaced polar angles. The 10 rings furthest upstream have 6 microphones per ring (equally spaced in the azimuthal direction and staggered from ring to ring), while the 5 rings furthest downstream have 4 microphones per ring. Errors in microphone positions are less than $0.1D$ based on photographic analysis.

3. THEORY

3.1. Acoustic projection method

Our approach is based on the concept of measuring pressure statistics just outside the jet shear layer to capture signatures of the large-scale turbulence. Microphones are configured to be sufficiently near the turbulent flow region to capture hydrodynamic pressure, yet far enough that non-linear source terms can be neglected. Under these conditions, the linear wave equation describes both the hydrodynamic pressure field (the source) and the acoustic wave propagation. It follows that the linear wave equation can be used to 'project' the source pressure to the acoustic field, and thereby relate dynamics of large-scale turbulence to noise generation.

We begin by developing an analytical solution for the Green's function G satisfying the reduced wave equation

$$\nabla_{\mathbf{x}}^2 G + k^2 G = \delta(\mathbf{x} - \mathbf{x}') \tag{1}$$

where $k = \omega/c$ is the acoustic wavenumber. In anticipation of applying Green's theorem, and since the surface-normal pressure gradient is unavailable from the measurements, we impose $G = 0$ on the near-field surface defined by the array. A spherical-polar coordinate system is used, centered on the virtual origin of the array, with polar angle θ and polar radius r. The angle θ is measured from the upstream (engine inlet) axis, and the near-field surface is given by $\theta = \theta_0$.

Introducing Fourier transforms in the azimuthal direction,

$$G_m = \frac{1}{2\pi}\int G(\phi)\mathrm{e}^{\mathrm{i}m\phi}d\phi \tag{2}$$

the wave equation becomes

$$\begin{aligned}&\frac{1}{r^2\sin\theta}\left[\sin\theta\frac{\partial}{\partial r}\left(r^2\frac{\partial G_m}{\partial r}\right)+\frac{\partial}{\partial\theta}\left(\sin\theta\frac{\partial G_m}{\partial\theta}\right)-\frac{m^2}{\sin\theta}G_m\right]\\&+k^2G_m=\frac{\delta(\theta-\theta')\delta(r-r')}{2\pi r^2\sin\theta}\mathrm{e}^{\mathrm{i}m\phi'}.\end{aligned} \tag{3}$$

It proves convenient to introduce the integral transform pair [46]

$$G_m(\nu,\theta) = \int_0^\infty G_m(r,\theta)H_{\nu+1/2}(kr)\frac{dr}{\sqrt{r}} \tag{4}$$

$$G_m(r,\theta) = -\frac{1}{2\sqrt{r}}\int_{-\mathrm{i}\infty}^{\mathrm{i}\infty}(\nu+1/2)G_m(\nu,\theta)J_{\nu+1/2}(kr)d\nu \tag{5}$$

obtained by applying the spectral representation method to the radial operator in the spherical wave equation. The Hankel functions are taken to be of the first kind, consistent with imposing the radiation condition at infinity for a $-\mathrm{i}\omega\mathrm{t}$ frequency convention. Applying (4) to both sides of (3) gives

$$\begin{aligned}&\left[\frac{1}{\sin\theta}\frac{\partial}{\partial\theta}\left(\sin\theta\frac{\partial G_m(\nu,\theta)}{\partial\theta}\right)+\left(\nu(\nu+1)-\frac{m^2}{\sin^2\theta}\right)G_m(\nu,\theta)\right]\\&=\frac{\delta(\theta-\theta')}{2\pi\sin\theta}\frac{1}{\sqrt{r'}}H_{\nu+1/2}(kr')\mathrm{e}^{\mathrm{i}m\phi'}\cdot\end{aligned}\tag{6}$$

Orthogonal eigenfunctions for the operator in (6) are given by the associated Legendre functions $P_\mu^m(\cos\theta)$, with eigenvalues μ determined by enforcing the boundary condition $P_\mu^m(\cos\theta_0)=0$. The solution for $G_m(\nu,\ \theta)$ can be written as an eigenfunction expansion

$$G_m(\nu,\theta)=\sum_\mu a_\mu P_\mu^m(\cos\theta)\tag{7}$$

where the coefficients a_μ are determined by applying the transform

$$\int_0^{\theta_0} f(\theta)P_\mu^m(\cos\theta)\sin\theta d\theta\tag{8}$$

to both sides of (6). We find

$$G_m(\nu,\theta)=\frac{\mathrm{e}^{\mathrm{i}m\phi'}}{2\pi\sqrt{r'}}\sum_\mu\frac{1}{A_\mu}\frac{H_{\nu+1/2}(kr')P_\mu^m(\cos\theta')P_\mu^m(\cos\theta)}{\{\nu(\nu+1)-\mu(\mu+1)\}}\tag{9}$$

where

$$A_\mu=\int_0^{\theta_0}\left|P_\mu^m(\cos\theta)\right|^2\sin\theta d\theta.\tag{10}$$

Applying (5) then gives

$$\begin{aligned}G_m(r,\theta)=&-\frac{1}{4\pi\sqrt{r}}\int_{-\mathrm{i}\infty}^{\mathrm{i}\infty}(\nu+1/2)\frac{\mathrm{e}^{\mathrm{i}m\phi'}}{\sqrt{r'}}\\&\times\sum_\mu\frac{1}{A_\mu}\frac{H_{\nu+1/2}(kr')P_\mu^m(\cos\theta')P_\mu^m(\cos\theta)}{\{\nu(\nu+1)-\mu(\mu+1)\}}J_{\nu+1/2}(kr)d\nu.\end{aligned}\tag{11}$$

The above integral representation applies for $r' > r$; this is the condition of primary interest since, upon applying Green's Theorem, integration of the near-field pressure will be over the 'observer' coordinates $\mathbf{x}$, and the acoustic far-field will correspond to the 'source' location $\mathbf{x}'$. The integral representation (11) is readily evaluated by closing the contour in the right half-plane and applying the residue theorem. We write

$$G_m(r,\theta) = g_m(r,\theta;r',\theta')\mathrm{e}^{\mathrm{i}m\phi'} \tag{12}$$

where

$$g_m(r,\theta;r',\theta') = \frac{\mathrm{i}}{4\sqrt{rr'}}\sum_{\mu}\frac{1}{A_\mu}H_{\mu+1/2}(kr')J_{\mu+1/2}(kr)P_\mu^m(\cos\theta')P_\mu^m(\cos\theta)\cdot \tag{13}$$

The above form was derived for $r' > r$, but it follows from the self-adjoint property of the wave equation that, for $r' < r$, the correct result is obtained by formally exchanging r and r' in (13).

Applying Green's Theorem, the acoustic field due to a pressure distribution on the near-field surface can be written

$$p_m(r',\theta') = 2\pi\sin\alpha\int_0^\infty p_m(r,\theta_0)\frac{\partial g_m}{\partial\theta}(r,\theta_0;r',\theta')dr \tag{14}$$

where α is the array spreading angle (cone half-angle). Using (14), the spectral density of the acoustic field can be expressed as

$$\begin{aligned} P_m(r',\theta',\omega) = 4\pi^2\sin^2\alpha\int\int R_m(r_1,r_2,\omega)\frac{\partial g_m}{\partial\theta}(r_2,\theta_0;r',\theta') \\ \times\left[\frac{\partial g_m}{\partial\theta}(r_1,\theta_0;r',\theta')\right]^* dr_1 dr_2 \end{aligned} \tag{15}$$

where

$$R_m \equiv \int\left\langle p_m^*(r_1,\theta_0,t)p_m(r_2,\theta_0,t+\tau)\right\rangle\mathrm{e}^{\mathrm{i}\omega\tau}d\tau \tag{16}$$

is the cross-spectral density of the near-field pressure, and (*) denotes complex conjugation.

3.2. Analytical source model

The pressure cross-spectrum R_m constitutes an equivalent acoustic source. We consider an analytical source model in the form of an amplitude-modulated traveling wave (wave-packet), qualitatively similar to an instability wave,

$$R_m(x_1, x_2, \omega) = (F(x_1)F(x_2))^{1/2} \exp[-(s / L_{cor}(\bar{x}))^2] e^{-2i\kappa(\bar{x})s} \tag{17}$$

where $\bar{x} = (x_1 + x_2)/2$ is the mean microphone location, $s = (x_1 - x_2)/2$ is the microphone half-separation, and $F(x)$ corresponds to the auto-spectral density along the array; κ and L_{cor} are the spatially varying wavenumber and correlation length scale, respectively. The orthogonal coordinates ($\bar{x}$, s) are convenient since they take advantage of the symmetry properties of the correlation. Note that in the present context R_m is defined as a function of the axial distance x from the nozzle trailing edge, whereas (16) was written in terms of the polar radius r along the array.

We introduce

$$F(x) = A(x / L_{src})^{\gamma-1} \exp(-\gamma x / L_{src}), \tag{18}$$

used previously by Glegg [47] in jet source models for far-field phased array studies. The length scale L_{src} characterizes the streamwise extent of the source region and A is the amplitude scale. For a wave-packet with $L_{cor} \ll L_{src}$ the correlation scale is small compared to the extent of the source region. Conversely, when L_{cor} is on the order of L_{src}, pressure is correlated over a scale comparable to the size of the source region. Although more general functions can be considered, we find that a simple linear model of the form

$$L_{cor}(\bar{x}) = B\bar{x} + C \tag{19}$$

provides a good representation of the data, while incorporating the physically realistic feature that the correlation scale increases with downstream distance from the nozzle exit.

4. RESULTS AND DISCUSSION

4.1. Identification of source model parameters

We next evaluate the equivalent source (16) using near-field array data for the jet operating conditions in Table 1, and use the results to identify parameters in the proposed source model. At each microphone ring, discrete Fourier transforms are applied in the azimuthal direction. Thus, for a given mode number m, a complex time series is associated with each of the 13 axial locations. In the following, we restrict our

Table 1: Jet operating conditions; $M_{jet} \equiv (U/a)_{jet}$, $M_\infty \equiv U_{jet}/a_\infty$ and Re $\equiv (\rho UD/\mu)_{jet}$.

Set pt.	M_∞ (M_{jet})	T_{jet}/T_∞	Re
SP27	0.90 (0.69)	1.76	4×10^5
SP46	0.90 (0.56)	2.70	2×10^5
SP29	1.33 (0.98)	1.76	6×10^5
SP141	1.58 (0.98)	2.70	4×10^5

attention to $m = 0$ and 1. For all cases, standard periodogram averaging methods are used to estimate the cross-spectral matrix R_m with a frequency bin size of $\Delta St = 0.05$, where $St \equiv fD/U_{jet}$.

Our algorithm for identifying the source model parameters proceeds as follows. First, measurements of the auto-spectral density (i.e. R_m evaluated at $x_1 = x_2$) are used to identify the parameters (A, L_{src},γ) in (18) using a non-linear least-squares method. Next, data for $|R_m|$ are used to determine parameters B and C in (19) using a global fit for all x_1 and x_2. Finally, phase data for the complex-valued R_m are used to determine the wavenumber $\kappa(\bar{x})$. Note that, for a given value of $\bar{x}$, determining κ represents a *linear* least-squares problem.

Results for the auto-spectral density (i.e. $F(x)$) are shown in figures 2 and 3 for $m =$ 0 and 1 respectively; corresponding model parameters are summarized in Table 2. The mean-square pressure along the array, normalized by its peak value, is plotted as a function of x/D for $St = 0.25$ and 0.40. At the low-speed condition for each temperature ratio (SP46 and SP27), the location of peak amplitude is at approximately 3-4 jet diameters, and pressure decays significantly before the last microphone ring. In contrast, pressure at the high-speed conditions (SP29 and SP141) peaks near the downstream-most microphone ring. This trend is consistent with the longer potential core of the higher-speed jets. Co-plotted for each combination of operating condition and frequency is the least-squares result for $F(x)$. The proposed model consistently provides a good representation of the near-field data; an exception is observed near the end of the array at the low-speed conditions (SP46 and SP27), where the data exhibit algebraic decay, much weaker than the exponential decay assumed in (18). This is due to acoustic contamination of the downstream portion of the array, the significance of which is discussed below.

It is important to establish that the near-field pressure is composed primarily of hydrodynamic fluctuations rather than acoustic radiation, since the goal is to devise a model linking large-scale turbulence and far-field sound (not merely to project acoustic radiation from one location to another). Peak pressure amplitudes, derived from the above curve fits, are plotted in figure 4 as a function of the acoustic Mach number $M_\infty \equiv U_{jet}/a_\infty$. Results are shown as pressure levels normalized to a bandwidth of unit Strouhal frequency, and referenced to $2 \times 10^{-5} Pa$. We see that the behavior with Mach number tends to follow a $p \propto M_\infty^2$ scaling expected for hydrodynamic disturbances.

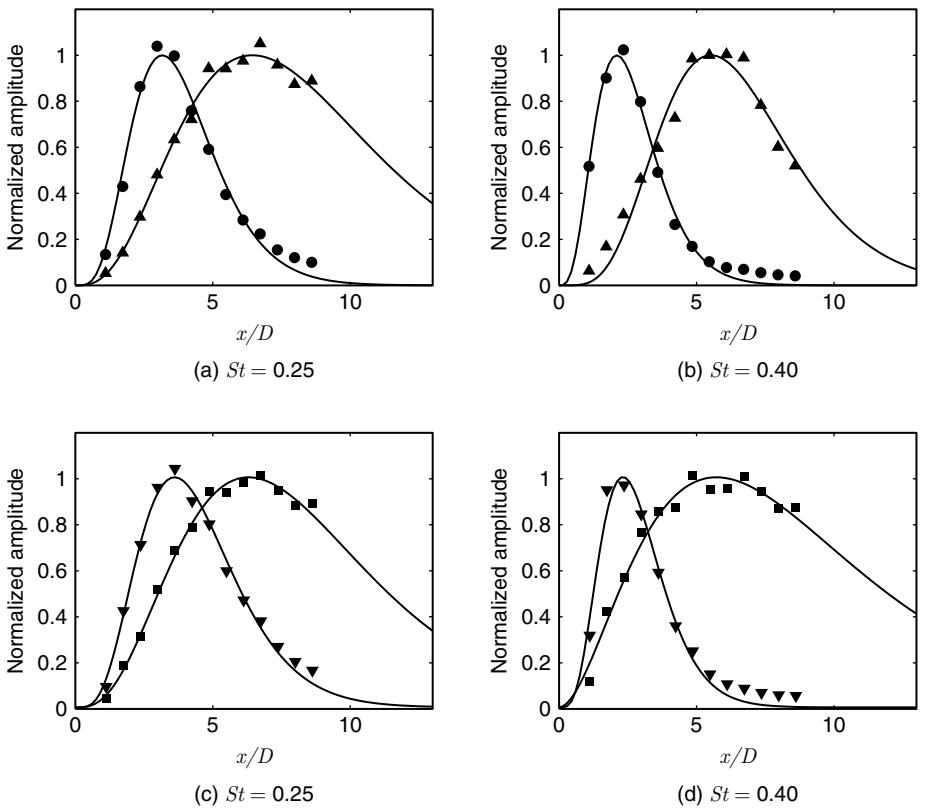

Figure 2: Measured wave-packet amplitude along array (symbols) compared to analytical model (——); SP141(▲), SP46(●), SP29(■), and SP27(▼); $m = 0$.

This observation is consistent with prior analysis of the current near-field array data reported by Suzuki and Colonius [38]. They demonstrated that pressure at each axial station of the array follows exponential (rather than algebraic) decay with radial distance from the jet centerline, consistent with being in the hydrodynamic near-field. For sufficiently large radii, algebraic decay, indicative of acoustic behavior, was found [38].

To further investigate the nature of the pressure field measured by the near-field array, we next consider the wave-packet phase speed. Representative results for the phase of R_m are shown in figures 5 and 6 as a function of microphone separation for $\bar{x} = 3$ and $\bar{x} = 6$, respectively. For a given value of frequency and mean microphone location, we see that the phase between microphones exhibits linear variation as assumed in (17). Thus, using a linear least-squares fit to determine the wavenumber κ, a phase speed can be defined according to $c_p(\bar{x}) = \omega/\kappa(\bar{x})$. Physically, this quantity represents the

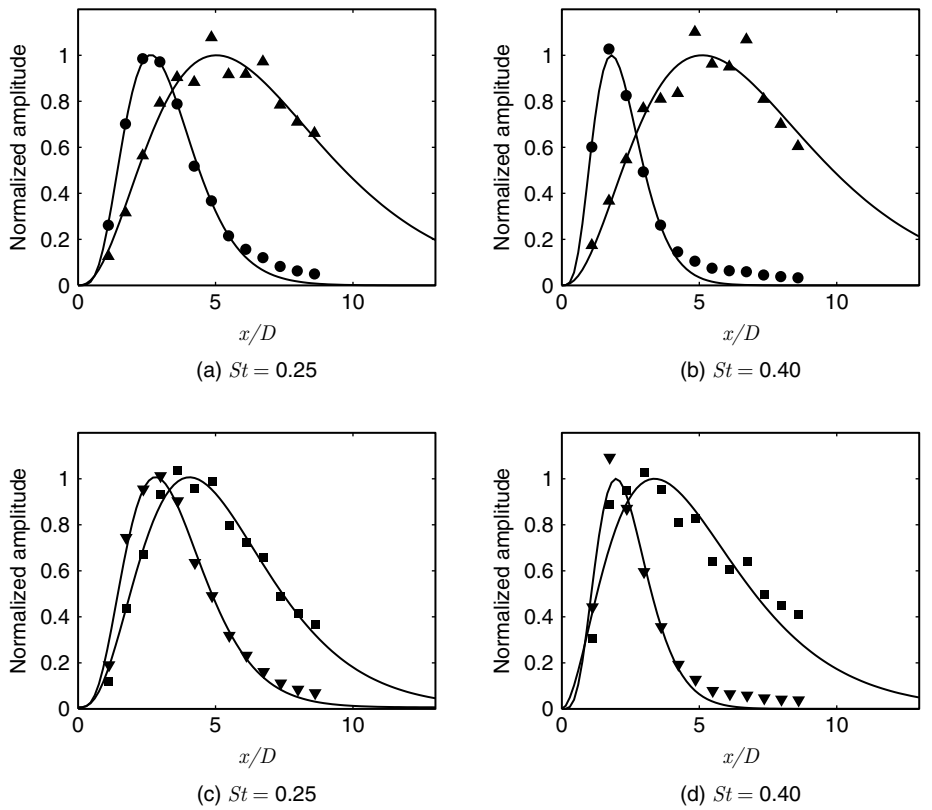

Figure 3: Measured wave-packet amplitude along array (symbols) compared to analytical model (——); SP141(▲), SP46(●), SP29(■), and SP27(▼); $m = 1$.

Table 2: Wave-packet amplitude parameters for $m = 0$.

Set pt.	St	$A[Pa^2/Hz]$	L_{src}/D	γ
SP27	0.25	7.74×10^2	4.44	5.36
	0.40	6.09×10^2	2.86	5.45
SP46	0.25	1.48×10^3	3.86	5.54
	0.40	4.25×10^2	2.67	4.77
SP29	0.25	8.49×10^2	8.24	4.25
	0.40	1.34×10^2	8.60	3.00
SP141	0.25	2.12×10^3	8.41	4.27
	0.40	1.65×10^4	6.56	6.37

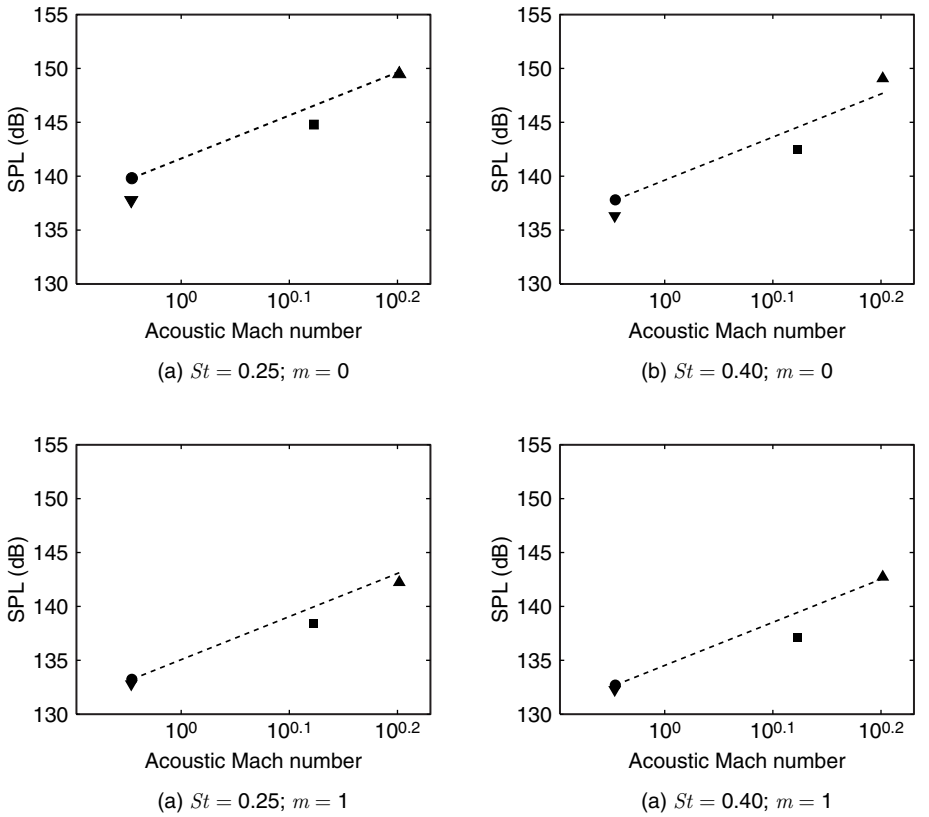

Figure 4: Peak pressure amplitude along array (symbols), compared to $p \propto M_\infty^2$ scaling (– – – –).

expected value of convection speed for the dominant flow (or acoustic) features most strongly correlated with a given location $\overline{x}$.

Phase speed distributions for each operating condition are shown in figures 7 and 8 for $m = 0$ and $m = 1$, respectively. For $m = 0$, phase speeds near the location of peak pressure amplitude from figure 2 are consistently in the neighborhood of $0.7\,U_{jet}$ across operating conditions; at $m = 1$ these values are slightly lower, in the range of $0.5\,U_{jet}$ to $0.6\,U_{jet}$. For SP27 and SP46, phase speeds near the location of peak amplitude are clearly subsonic relative to a_∞, and therefore representative of non-acoustic disturbances. For SP29 and SP141, separation of hydrodynamic and acoustic phenomena on the basis of phase speed is more tenuous, since c_p is (marginally) supersonic. However, the observation that the phase speed scales with jet velocity (near

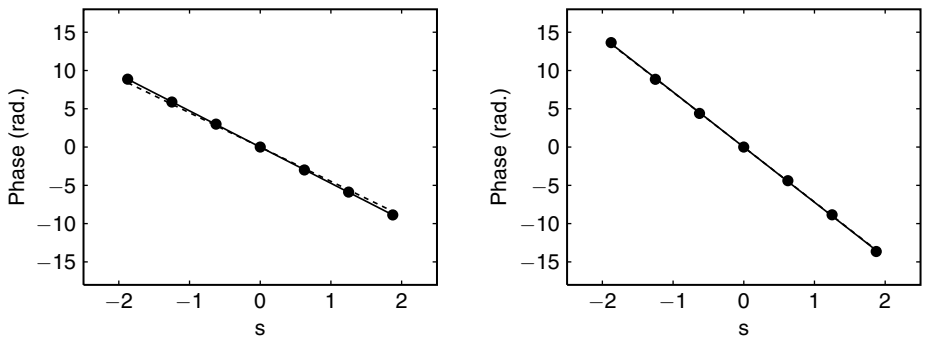

Figure 5: Measured wave-packet phase for SP46 (•) compared to linear model (——). Phase variation corresponding to $0.7U_{jet}$ shown for reference (– – – –); $m = 0$, $\bar{x} = 3$.

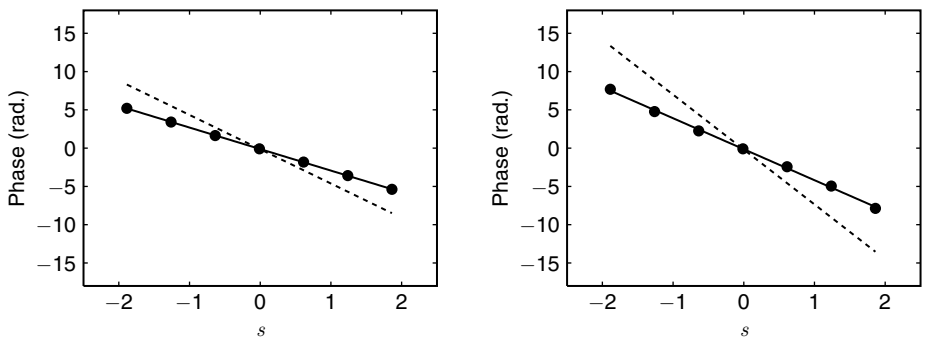

Figure 6: Measured wave-packet phase for SP46 (•) compared to linear model (——). Phase variation corresponding to $0.7U_{jet}$ shown for reference (– – – –); $m = 0$, $\bar{x} = 6$.

the wave-packet peak) suggests that hydrodynamic events are indeed dominant for both the high- and low-speed conditions.

For SP27 and SP46, phase speed increases markedly toward the downstream region of the array. This characteristic is most pronounced at $m = 1$ (figure 8). Phase speeds in excess of U_{jet} are clearly indicative of acoustic signatures in the near-field pressure. This is consistent with the algebraic pressure decay noted previously in the discussion of figures 2 and 3. For the high-speed jets (SP29 and SP141), the phase

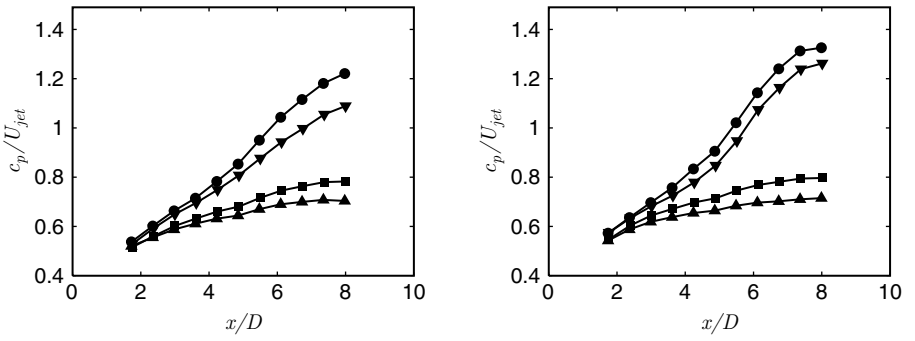

(a) $St = 0.25$; $m = 0$ (b) $St = 0.40$; $m = 0$

Figure 7: Normalized phase speed as function of $\bar{x}$; SP141(▲), SP46(●), SP29(■), and SP27(▼); $m = 0$.

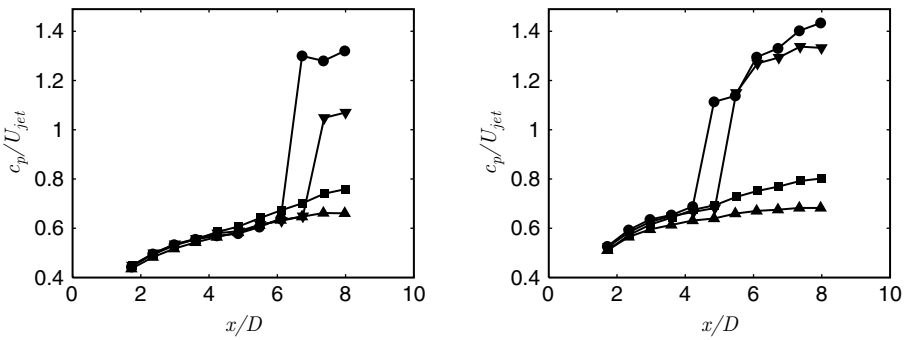

(a) $St = 0.25$; $m = 1$ (b) $St = 0.40$; $m = 1$

Figure 8: Normalized phase speed as function of $\bar{x}$; SP141(▲), SP46(●), SP29(■), and SP27(▼); $m = 1$.

speed exhibits a similar monotonic increase with downstream distance, but remains lower than the jet speed.

We next compare measurements of R_m against the model (17) as a function of x_2 for fixed values of x_1. Representative results are shown in figures 9 and 10 for $x_1/D = 3$ and $x_1/D = 6$, respectively. These results clearly illustrate the wave-like structure of the source, and its appreciable correlation over several jet diameters, consistent with the notion of large-scale turbulence. Agreement between model and data is consistently good across operating condition and frequency. The only significant discrepancy is seen in figure l0d for SP46; in this case, the reference microphone location x_1 is in the 'tail' of the wave-packet (see figure 2b), where pressure amplitudes are quite small relative to the wave-packet peak, and the model for *F(x)* imposes significant error due to its exponential decay.

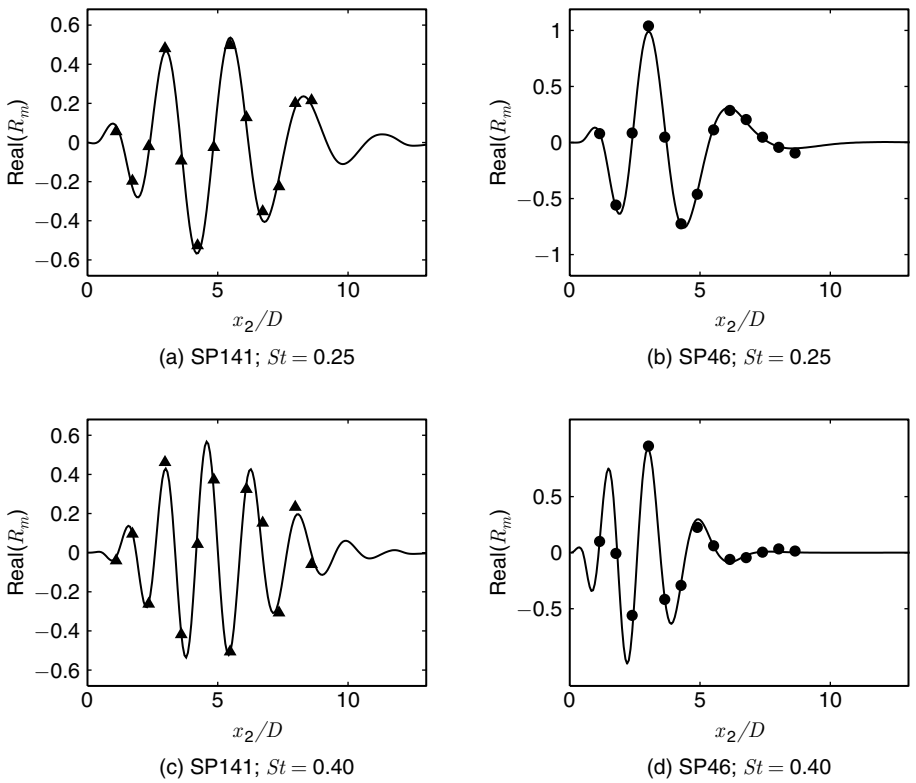

Figure 9: Real part of measured $R_m(x_1,\ x_2)$ (symbols) compared to wave-packet model (——) for reference microphone at $x_1/D = 3$; $m = 0$.

4.2. Acoustic projection results

We next use the equivalent source (16) and projection method (15) to reconstruct the acoustic field for operating points in table 1, and compare results against the acoustic array data. Since the acoustic array has only four microphones on each of the downstream-most axial rings, we restrict our attention to azimuthal modes $m = 0$ and 1. Sound pressure levels are presented as spectral densities using a reference of $(2 \times 10^{-5})^2 Pa^2/Hz$.

It is apparent in figures 2 and 3 that the wave-packets extend downstream of the last near-field microphone ring, particularly for the high-speed operating points SP141 and SP29. To avoid spurious wave-packet truncation effects, our acoustic calculation is based on the analytical source model (17) with parameters identified from the near-field data, as discussed above. Thus, wave-packets are extrapolated beyond the last microphone ring according to the exponential function (18). For $\bar{x}$ outside the available data, we set $c_p(\bar{x})$ equal to the last measured value. For all results presented here, source wave-packets have been extrapolated to $x/D = 40$, minimizing any domain truncation effects.

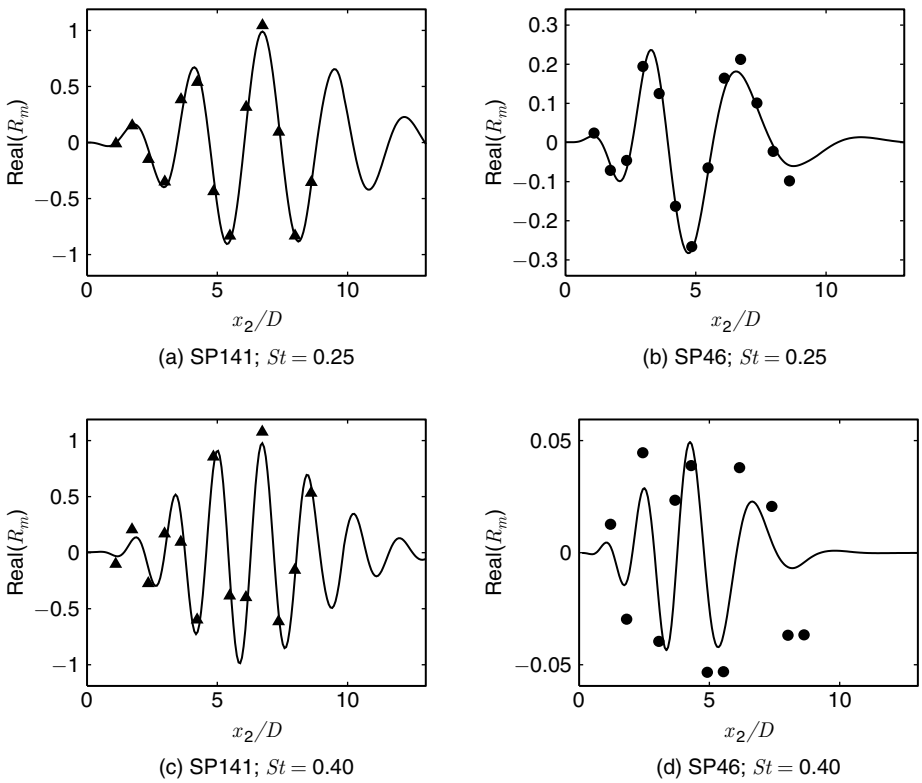

Figure 10: Real part of measured $R_m(x_1, x_2)$ (symbols) compared to wave-packet model (——) for reference microphone at $x_1/D = 6$; $m = 0$.

Comparisons between acoustic array data and the wave-packet model are shown in figures 11 and 12 for $m = 0$ and $m = 1$, respectively. We emphasize that comparisons are made on the basis of absolute levels, with no amplitude adjustments. We focus our discussion first on the high-speed operating points SP141 and SP29. At $m = 0$, the acoustic pressure data exhibit a pronounced directivity peak near 140°. This is a well-known feature of high-speed jet noise, and has been used by Tam et al. [19] to support the argument for two distinct source mechanisms: 'fine scale' turbulence noise characterized by a relatively uniform directivity, and 'large scale' turbulence noise having a distinct peak at aft angles. Note that the amplitude and lobe width of this aft directivity peak is captured very well by the model. Moreover, comparison of figures lla and 11b shows that the wave-packet model captures the distinct narrowing of the directivity peak as frequency increases from $St = 0.25$ to $St = 0.40$. The wave-packet directivity pattern is qualitatively consistent with the two-source hypothesis, having a rapid roll-off with decreasing angle, and thus under-predicting the acoustic measurements near side angles where fine scale turbulence noise is expected to dominate.

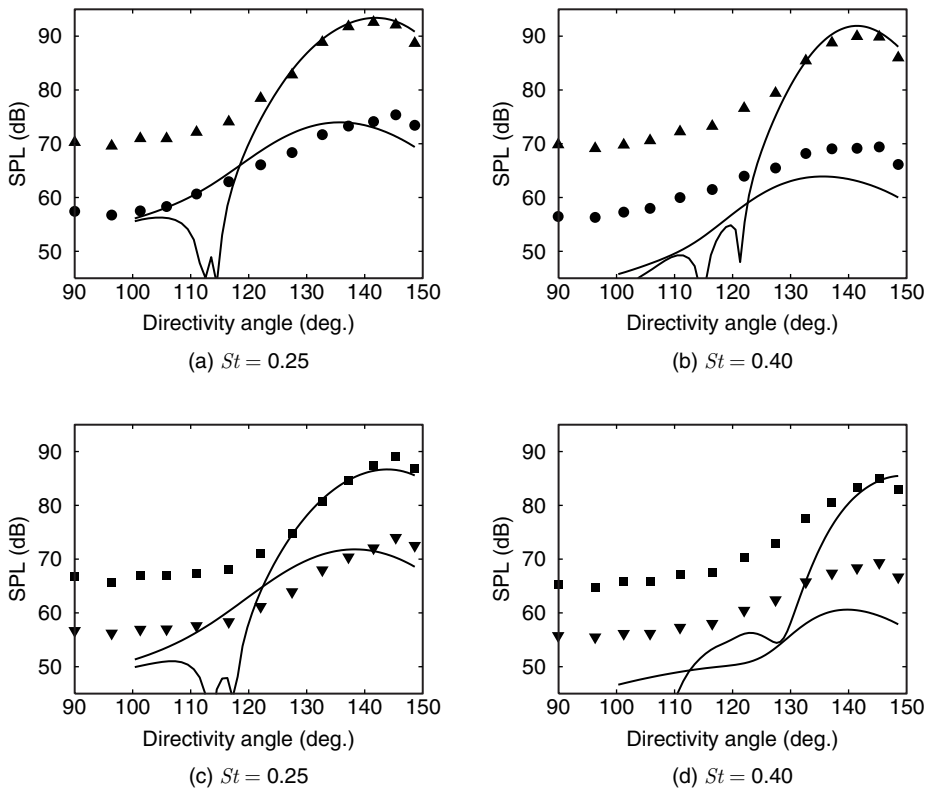

Figure 11: Comparison of measured (symbols) and projected(——) sound pressure along acoustic array for SP141(▲), SP46(●), SP29(■), and SP27(▼); $m = 0$.

Corresponding results for $m = 1$ are shown in figure 12. Measured sound pressure levels at the peak directivity angle are roughly 10 dB lower than those for $m = 0$, while levels at lower angles are roughly the same, resulting in a much less pronounced directivity peak. We see that the wave-packet model provides a good prediction of the measured trend between $m = 0$ and $m = 1$ for the aft most angles.

Discrepancies between the wave-packet model and data are generally larger for the low-speed operating points SP46 and SP27; in these cases, under-prediction of the acoustic pressure might be expected based on the two-source hypothesis, since the lower-speed jets would tend to have some contribution from the fine-scale source even at aft angles, particularly away from the peak frequency of the large-scale turbulence source. This, however, does not account for the over-prediction seen for SP27 and SP46 at $St = 0.25$ (i.e. figures lla,c); peak levels, as well as the shape of the aft directivity pattern, appear to be well predicted, but the peak angle is under-predicted by approximately 10°. We speculate this discrepancy can be attributed to the exponential

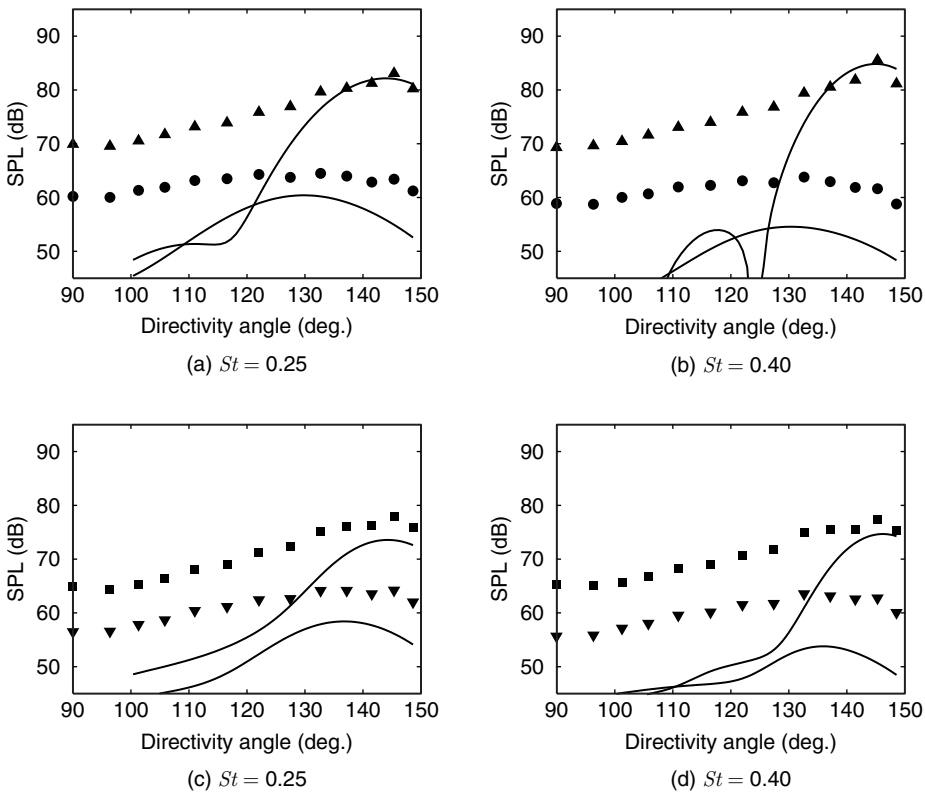

Figure 12: Comparison of measured (symbols) and projected (——) sound pressure along acoustic array for SP141(▲), SP46(●), SP29(■), and SP27(▼); $m = 1$.

decay imposed by the model (18), which is inconsistent with the algebraic decay seen in the data (see section 4.1). This region of weaker algebraic decay has finite correlation with the peak of the wave-packet and thus, at least in part, represents the acoustic footprint of the upstream-generated radiation. Part of this acoustic signature might also be attributed to fine scale mixing, or other sources not correlated with the wave-packet source. In any case, imposing the exponential decay has the effect of artificially modifying the impedance along the near-field surface sensed by acoustic rays emanating from the hydrodynamic wave-packet.

Assuming that the source characteristics (i.e. the hydrodynamic wave-packet) are largely preserved by the windowing, we would expect the total power output to be approximately conserved, despite the inaccurate boundary condition downstream of the dominant source region. This appears to be consistent with the results shown in figures 11a and 11c, where discrepancies between the acoustic array data and wave-packet model might be explained as a simple shift in the peak directivity angle toward smaller inlet angles, with approximate preservation of total acoustic power.

The windowing error can also be described in terms of wavenumber filtering. Although the impact of the spatial window is in some sense small relative to the peak amplitude of the wave-packet, we note that sensitivity of the acoustic projection to such effects increases with decreasing jet speed. This can be understood by recalling that the effect of the spatial window is a convolution of the true near-field wavenumber spectrum with that of the window function. Thus, at low speeds, where the propagating wavenumbers are at the 'tails' of the wave-packet spectrum, the convolution effect can be significant. Conversely, we expect the impact of neglecting the algebraic tails of the wave-packet to be relatively small for sufficiently high-speed jets.

Despite discrepancies noted above for the low-speed cases, overall agreement between wave-packet model and acoustic measurements is good, particularly given the 20 dB range of peak sound pressure levels represented by the current set of jet operating

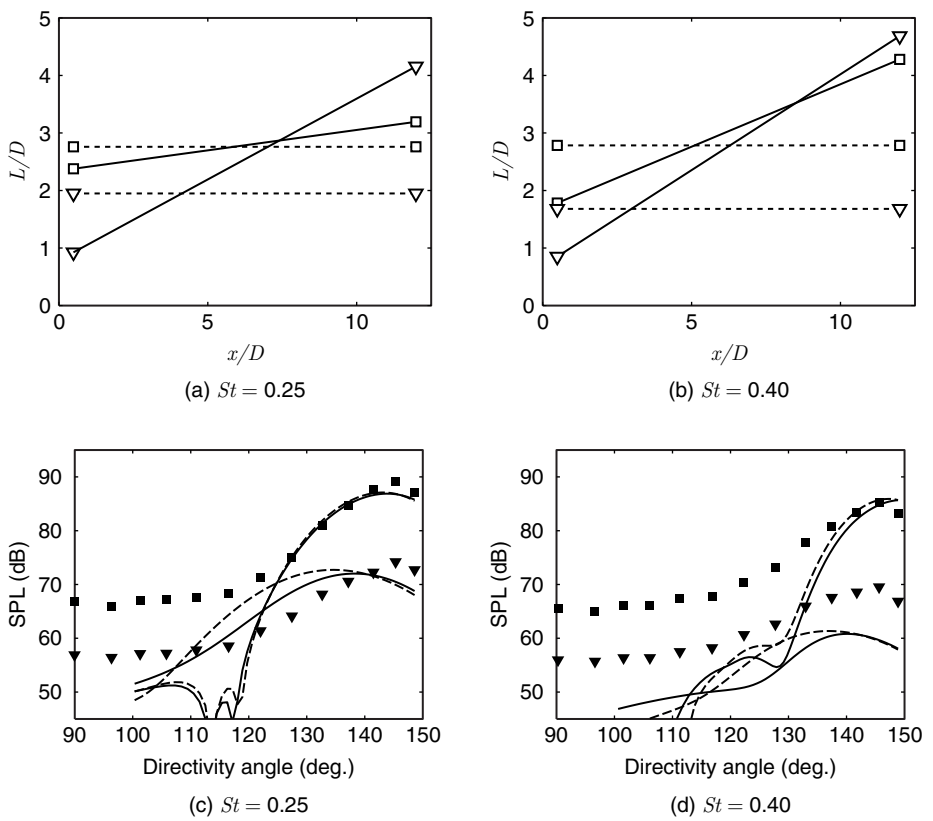

Figure 13: Length scale distributions and corresponding projection results for two-parameter model (——) compared to uniform length scale model (– – – –) for SP29(■) and SP27(▼); $m = 0$.

points. We have shown that the model captures trends in peak amplitude and azimuthal mode balance as a function of operating condition, and thus appears to capture salient features of the source mechanisms controlling low-frequency aft-angle sound generation by large-scale turbulence.

An obvious concern is sensitivity of the acoustic results to selection of model parameters. Since much of the fitting involves non-linear least-squares methods, the model parameters are non-unique, and have some inherent uncertainty. Our studies to date have shown that, for the high-speed cases, radiation in the aft angles (beyond approximately 130°) is quite robust to typical variability encountered in the curve fitting. In general, the largest sensitivities are observed at side angles, and for low speeds; a comprehensive study is beyond the current scope, and will be reported in a forthcoming-paper. In order to provide some notion of the sensitivity, figure 13 compares acoustic projection results obtained using the length scale model (19) to those obtained by assuming a constant length scale (i.e. enforcing the constraint $B = 0$ in equation (19)). In both cases, the length scale parameters have been selected to provide the best fit in a least-squares sense. The resulting length scale distributions are shown in figures 13a and 13b, and the corresponding projection results are shown in figures 13c and 13d. The low-speed operating point SP27 exhibits the largest variability of roughly 5 dB, while SP29 shows significantly less variation of 1–2 dB. In all cases, general features such as peak levels and shape of the directivity lobes are seen to be very robust. Note that the corresponding changes in length scale are significant, and larger than typical variations associated with uncertainty in the curve fitting process.

5. CONCLUSIONS AND FUTURE WORK

A wave-packet based modeling framework has been developed for noise generation by large-scale turbulence in jets. Our approach is based on the concept of measuring pressure sufficiently near the jet turbulent shear layer so that signatures of hydrodynamic disturbances are dominant, yet sufficiently far such that the effects of non-linearity and non-uniform mean flow can be neglected. We define an equivalent acoustic source using the two-point space-time correlation of near field pressure, and relate this to the acoustic field by solving the linear uniform-medium wave equation. Results show that the equivalent source can be described by a simple parametric model having the form of a Gaussian wave packet with an algebraic-exponential axial distribution of the pressure auto-spectrum. The model is found to provide a robust representation of near-field pressure data for subsonic jets over a range of operating points encompassing both subsonic and supersonic acoustic Mach numbers. Overall agreement between the measured acoustic field and that calculated from the wave-packet source model is very encouraging; the model captures trends in peak amplitude and azimuthal mode balance as a function of operating condition. In general, the predicted radiation characteristics are consistent with the two-source hypothesis originated by Tam et al. [19]. We find that the wave-packet source is indeed ‘large scale’, having correlation length scales on the order of jet diameters, and that the wave-packet model tends to significantly under-predict radiation to side angles, where fine

scale turbulence would be expected to dominate. Moreover, the results presented here provide compelling evidence that large-scale wave-like structures, known to dominate aft radiation in supersonic jets, are also relevant in subsonic jets.

We conclude that the proposed model captures salient features of fundamental source mechanisms controlling low-frequency aft-angle sound generation by large-scale turbulence. Ongoing efforts are aimed at exercising the model in a parametric fashion to better understand how source characteristics control aft-angle jet noise. This will aid in a better understanding of the sensitivity of the sound field to changes in the flow structure evolution.

In its present form the model lacks first-principles predictive capability. Thus, efforts are underway to correlate the source parameters using aerodynamic quantities such as potential core length. We are also extending linear stability theory, already shown to reasonably well represent the observed wave packet structure over the initial 4–5 diameters of the jet [38], to account for nonparallel effects and nonlinearity that is important further downstream. Non-linear Parabolized Stability Equations (NPSE) appear to be well suited for this purpose [48, 49]. Finally, it remains to be assessed whether wave packet amplitudes can be predicted with sufficient accuracy to constitute a quantitatively accurate model describing sound generation by large-scale turbulence. However, the level of agreement demonstrated in this paper makes clear that this approach offers an alternative to the traditional acoustic analogy approach that is more intuitively connected with large-scale turbulence, and may offer better insight for effective noise suppression strategies.

ACKNOWLEDGMENTS

The authors are indebted to Drs. J. Bridges and S.-S. Lee for generously sharing their data and for fruitful discussions. Tim Colonius gratefully acknowledges the support of a grant from the Aeroacoustics Research Consortium (AARC) of the Ohio Aerospace Institute. We also wish to thank Dr. R. Schlinker for technical discussions and support.

REFERENCES

[1] Bodony, D.J. & Lele, S.K., "Review of the current status of jet noise prediction using large-eddy simulation," AIAA Paper 2006-0486, 2006.

[2] Lighthill, M.J., "On sound generated aerodynamically: I. General theory," *Proc. R. Soc. Lond., Series A,* Vol. 211, 1952, pp. 564–587.

[3] Lilley, G.M.,"On the noise from jets," AGARD CP-131, 1974.

[4] Balsa, T.F. & Gliebe, P.R., "Aerodynamics and noise of coaxial jets," *AIAA Journal,* Vol. 15, No. 11, 1977, pp. 1550–1558.

[5] Khavaran, A., Krejsa, E.A. & Kim, C.M., "Computation of supersonic jet mixing noise from an axisymmetric convergent-divergent nozzle," *Journal of Aircraft,* Vol. 31(3), 1994, pp. 603–609.

[6] Khavaran, A., "Role of anisotropy in turbulent mixing noise," *AIAA Journal,* Vol. 37(7), 1999, pp. 832–841.

[7] Tam, C. K. W. & Auriault, L., "Jet mixing noise from fine-scale turbulence," *AIAA Journal,* Vol. 37(2), 1999, p. 145–153.

[8] Tam, C. K. W. & Pastouchenko, N. N., "Fine scale turbulence noise from dual stream jets," *AIAA Journal,* Vol. 44(1), 2006, pp. 90–101.

[9] Mollo-Christensen, E., "Jet noise and shear flow instability seen from an experimenter's viewpoint," *ASME Journal of Applied Mechanics,* Vol. 34, 1967, pp. 1–7.

[10] Liu, J.T.C., "Developing large-scale wavelike eddies and the near jet noise field," *J. Fluid Mech.,* Vol. 62, 1974, pp. 437–464.

[11] Mankbadi, R.R. & Liu, J.T.C., "A study of the interaction between large-scale coherent structures and fine-grained turbulence in a round jet," *Phil. R. Soc. Lond. Series A,* Vol. 298, 1981, pp. 541–602.

[12] Mankbadi, R.R., "On the interaction between fundamental and sub-harmonic instability waves in a turbulent round jet," *J. Fluid Mech.,* Vol. 160, 1985, pp. 385–419.

[13] Morris, P.J., Giridharan, G.M. & Lilley, M.G., "On the turbulent mixing of compressible free shear layers," *Proc. R. Soc. Lond.,* A 431, 1990, pp. 219–243.

[14] Tam, C.K.W., "Jet Noise: Since 1952," *Theor. Comp. Fluid Dynamics,* Vol. 10, 1998, pp. 393–405.

[15] Tam, C.K.W. & Morris, P.J., "The radiation of sound by the instability waves of a compressible plane turbulent shear layer," *J. Fluid Mech.,* Vol. 98, 1980, pp. 349–381.

[16] Tam, C.K.W. & Burton, D.E., "Sound generated by instability waves of supersonic flows. Part 1: Two-dimensional mixing layers," *J. Fluid Mech.,* Vol. 138, 1984, pp. 249–271.

[17] Tam, C.K.W. & Burton, D.E., "Sound generated by instability waves of supersonic flows. Part 2: Axisymmetric jets," *J. Fluid Mech.,* Vol. 138, 1984, pp. 273–295.

[18] Wu, X., "Mach wave radiation of nonlinearly evolving supersonic instability modes in shear layers," *J. Fluid Mech.,* Vol. 523, 2005, pp. 121–159.

[19] Tam, C.K.W., Golebiowski, M. & Seiner, J.M., "On the two components of turbulent mixing noise from supersonic jets," AIAA Paper 96–1716, 1996.

[20] Tam, C.K.W., Viswanathan, K., Ahuja, K.K. & Panda, J., "The sources of jet noise: experimental evidence," AIAA Paper 2007-3641, 2007.

[21] Morris, P.J., "A note on noise generation by large scale turbulent structures in subsonic and supersonic jets," *International Journal of Aeroacoustics,* Vol. 8(4), 2009, pp. 301–315.

[22] Siddon, T.E., "Noise source diagnostics using causality correlations," AGARD CP 131, Noise Mechanisms, 1973, pp. 7–1:7–13.

[23] Lee, H.K. & Ribner, H.S., "Direct correlation of noise and flow in a jet," *Journal of the Acoustical Society of America,* Vol. 52(5), 1972, pp. 1280–1290.

[24] Seiner, J.M. & Reethof, G., "On the distribution of source coherency in subsonic jets," AIAA paper 74-4, 1974.

[25] Panda, J., Seasholtz, R.G. & Elam, K.A., "Investigation of noise sources in high-speed jets via correlation measurements," *J. Fluid Mech.,* Vol. 537, 2005, pp. 349–385.

[26] Bridges, J. & Wernet, M.P. "Turbulence measurements of separate flow nozzles with mixing enhancement features," AIAA Paper 2002-2484, 2002.

[27] Bridges, J. & Wernet, M. "Measurements of the aeroacoustic sound source in turbulent jets," AIAA 2003–3130, 2003.

[28] Hileman, J., Thurow, B. & Samimy, M., "Acoustic source localization using a 3-D microphones array in a Mach 1.3 jet," AIAA 2002–0366, 2002.

[29] Hileman, J., Thurow, B., Caraballo, E. & Samimy, M., "Large-scale structure evolution and sound emission in high-speed jets; real-time visualization with simultaneous acoustic measurements," *J. Fluid Mech.,* Vol. 544, 2005, pp. 277–307.

[30] Arndt, R.E.A, Long, D.F., Glauser, M.N., "The proper orthogonal decomposition of pressure fluctuations surrounding a turbulent jet," *J. Fluid Mech.,* Vol. 340, 1997, pp. 1–33.

[31] Freund, J.B & Colonius. T., "POD analysis of sound generation by a turbulent jet," AIAA Paper 2002-0072, 2002.

[32] Freund, J.B., & Colonius, T., "Turbulence and sound-field POD analysis of a turbulent jet," *International Journal of Aeroacoustics,* Vol. 8(4), 2009, pp. 337–354.

[33] Ukeiley, L.S. & Ponton, M.K., "On the near field pressure of a transonic axisymmetric jet," *International Journal of Aeroacoustics,* Vol. 3(1), 2004, pp. 43–66.

[34] Picard, C. & Delville, J., "Pressure velocity coupling in a subsonic round jet," *Intl. J. of Heat and Fluid Flow,* Vol. 21(3), 2000, pp. 359–364.

[35] Tinney, C.E., Ukeiley, L.S. & Glauser, M.N., "Low-dimensional characteristics of a transonic jet. Part 2. Estimate and far-field prediction," *J. Fluid Mech.,* Vol. 615, 2008, pp. 53–92.

[36] Kerherve, F., Guitton, A., Jordan, P., Delville, J., Fortune, V., Gervais, Y. & Tinney, C., "Identifying the dynamics underlying the large-scale and fine-scale jet noise similarity spectra," AIAA Paper 2008-3027, 2008.

[37] Tinney, C.E. & Jordan, P., "The near pressure field of co-axial subsonic jets," *J. Fluid Mech.,* Vol. 611, 2008, pp. 175–204.

[38] Suzuki, T. & Colonius, T. "Instability waves in a subsonic round jet detected using a near-field phased microphone array," *J. Fluid Mech.,* Vol. 565, 2006, pp. 197–226.

[39] Crighton, D.G. & Huerre, P., "Shear-layer pressure fluctuations and superdirective acoustic sources," *J. Fluid Mech.,* Vol. 220, 1990, pp. 355–368.

[40] Laufer, J. & Yen, T.C., "Noise generation by a low-Mach-number jet," *J. Fluid Mech.,* Vol. 134, 1983, pp. 1–31.

[41] Fuchs, H.V., "Space correlations of the fluctuating pressure in subsonic turbulent jets," *J. Sound and Vibration,* Vol. 23(1), 1972, pp. 77–99.

[42] Michalke, A., "Effect of spatial source coherence on the radiation of jet noise," *J. Sound and Vibration,* Vol. 55(3), 1977, pp. 377–394.

[43] Suzuki, T. & Colonius, T., "Relation between instability waves and low-frequency jet noise investigated with phased microphone arrays," AIAA Paper 2006-622, 2006.

[44] Brown, C. & Bridges, J., "Small hot jet acoustic rig validation," NASA TM-2006-214234, 2006.

[45] Tanna, H.K. "Experimental-study of jet noise: 1. Turbulent mixing noise," *J. Sound and Vibration* Vol. 50(3), 1977, pp 405–428.

[46] Dudley, D.G., *Mathematical foundations for electromagnetic theory*. IEEE Press, 1994.

[47] Glegg, S., Ph. D. Thesis, University of Southampton, 1979.

[48] Cheung, L.C, Bodony, D.J. & Lele, S.K., "Noise radiation predictions from jet instability waves using a hybrid nonlinear PSE-acoustic analogy approach," AIAA Paper 2007-3638, 2007.

[49] Gudmundsson, K., Colonius, T., "Parabolized stability equation models for turbulent jets and their radiated sound," AIAA Paper 2009-3380, 2009.